

Fractional Spin fluctuations and quantum liquid signature in $\text{Gd}_2\text{ZnIrO}_6$

Birender Singh^{1#}, D. Kumar¹, V. Kumar¹, M. Vogl², S. Wurmehl^{2,3}, S. Aswartham², B.

Büchner^{2,3} and Pradeep Kumar^{1*}

¹*School of Basic Sciences, Indian Institute of Technology Mandi, Mandi-175005, India*

²*Leibniz-Institute for Solid-State and Materials Research, IFW-Dresden, 01069 Dresden, Germany*

³*Institute of Solid-State Physics, TU Dresden, 01069 Dresden, Germany*

Abstract:

Hitherto, the discrete identification of quantum spin liquid phase, holy grail of condensed matter physics, remains a challenging task experimentally. However, the precursor of quantum spin liquid state may reflect in the spin dynamics even in the paramagnetic phase over a wide temperature range as conjectured theoretically. Here we report comprehensive inelastic light (Raman) scattering measurements on the Ir based double perovskite, $\text{Gd}_2\text{ZnIrO}_6$, as a function of different incident photon energies and polarization in a broad temperature range. Our results evidenced the spin fractionalization within the paramagnetic phase reflected in the emergence of a polarization independent quasi-elastic peak at low energies with lowering temperature. Also, the fluctuating scattering amplitude measured via dynamic Raman susceptibility increases with lowering temperature and decreases mildly upon entering into long-range magnetic ordering phase, below 23 K, suggesting the magnetic origin of these fluctuations. This anomalous scattering response is thus indicative of fluctuating fractional spin evincing the quantum spin liquid phase in a three-dimensional double perovskite system.

#email id: birender.physics5390@gmail.com

**email id: pkumar@itmandi.ac.in*

Quantum spin liquid (QSL), a state sans long-range magnetic ordering owing to strong quantum fluctuations but favors entanglement of spins even over a long-range, has been very fascinating since it was proposed in the 1970s [1]. QSL state, a holy grail which so far has been elusive, is most sought after by the contemporary scientific community. A large number of systems have been proposed to be potential host for these elusive states despite some having long-range ordering at low temperature [2-4] with arguments that precursor of QSL state may emerge even in the paramagnetic phase over a wide temperature range owing to the dynamic quantum fluctuations associated with a complex interplay of spin and orbital degrees of freedom (DoF) [5-8]. Recently, the search has been extended to iridium-based oxides, and quite interestingly even to the rare earth systems [9-15]. In iridium-based oxides the focus is on double perovskites (DP), such as $A_2B\text{IrO}_6$, ($A = \text{La, Nd, Sm, Gd}$; $B = \text{Zn, Cu, Mg}$), despite of the fact that these systems do show long-range magnetic ordering at low temperature. The existence of QSL state may be inferred indirectly from light scattering experiments via the observation of a broad continuum instead of sharp magnetic modes, characteristic of a long-range ordered phase [7, 9-11, 16].

The iridium-based DP system have an intertwined spin, orbital, and lattice DoF along with coupled crystalline electric field, and the physics of Ir^{4+} ($5d^5$) DP system is believed to be driven by spin-orbital entangled $J_{\text{eff}} = 1/2$ state [17-19]. Interestingly, in these systems the relativistic spin-orbit coupled $J_{\text{eff}} = 1/2$ iridium moments reside on the 3D geometrically frustrated face-centered cubic lattice providing unique symmetry allowed anisotropic interactions leading to the Kitaev type interactions suggesting these DP as potential QSL candidate [13-14] despite having a long-range ordering at low temperature. The effective Hamiltonian with multiple interactions is given as $H = \sum_{i,j} J_k S_i^\alpha S_j^\alpha + J \vec{S}_i \vec{S}_j$ [13], where J_k and J are the Kitaev and Heisenberg parameters, respectively; α is component of the spin directed perpendicularly to the bond

connecting spins (i, j) , and the ground state, $|GS\rangle$, with this model Hamiltonian is found to be A-type antiferromagnet incommensurate with the experiments [13]. In case of $5d$ system, the strong spin-orbit coupling (SOC) is expected to quench the orbital DoF, and only spin channel are considered to be active. However, it has been advocated that even in case of $5d$ system the Jahn-Teller mechanism does effect t_{2g} orbitals in spite of the strong SOC [20-21], thus suggesting non-zero contribution of orbital DoF in controlling the physics of these system. In fact, a spin-orbital entangled quantum liquid state is reported in another iridium-based system suggesting the crucial role of these DoF [22]. The system under study, DP $\text{Gd}_2\text{ZnIrO}_6$, undergo a magnetic transition at ~ 23 K (T_N) with a canted antiferromagnetic ordering attributed to the interplay between Gd and Ir magnetism, and the transport measurements also evinced the signature of incoherent spin fluctuations [23]. The crystalline electric field ground state (${}^8S_{7/2}$) of Gd^{3+} is composed of Kramer's doublets which allows quantum tunneling owing to sizable component of $|J, J_z\rangle$ with a small $|J_z\rangle$ and is well separated from the first excited state, therefore providing a way to realize the QSL state [15, 24, 25] in these rare-earth system as suggested recently.

Motivated by these concrete suggestions for a possible QSL state in these iridium-based DP system, we undertook an in-depth inelastic light (Raman) scattering studies to probe the quasiparticle excitations in $\text{Gd}_2\text{ZnIrO}_6$, with Ir^{4+} ($5d^5$), where the physics is governed by the $J_{\text{eff}}=1/2$ picture. Smoking gun evidence for a QSL phase may be uncovered via the observation of a quantum spin and/or orbital fluctuations, and these dynamic fluctuations may reveal itself indirectly via interacting with the photon which is inelastically scattered by these underlying quantum fluctuations. Since the QSL state is a manifestation of the topological order,

it does not break any symmetry, and so the translational one is characterized by zero momentum, it is expected that Raman spectroscopy can be a suitable technique to detect signature of a QSL state. Raman scattering is a very powerful technique to probe the dynamical quantum fluctuations associated with spin and orbital DoF reflected via the emergence of the quasi-elastic peaks at low energy in the Raman response $\chi''(\omega, T)$ [26-32], smoking gun of a quantum spin liquid state. The unique ability of Raman scattering in the present study is reflected in the observation of a strong quasi-elastic response with lowering temperature, quite startling it start emerging much above the long-range magnetic ordering temperature. The low energy quasi-elastic peak is found to be nearly isotropic with respect to the polarization of light fixed in the basal plane and is consistent with the constraints imposed by the symmetry. This characteristic low energy scattering response clearly evince the presence of strong spin-orbital coupled underlying quantum fluctuations which survive even much above the T_N . Quite interestingly, the corresponding estimated dynamic Raman susceptibility, $\chi^{dyn}(T)$, amplitude does not quenched below T_N , instead it decreases only by $\sim 25\%$ of its maximum value, as expected for a conventional magnetic system, signaling that it emerges from a quantum liquid state.

Raman scattering measurements on $\text{Gd}_2\text{ZnIrO}_6$ polycrystalline, synthesized as described in ref. 23, samples were performed in quasi-back scattering configuration using 532-nm and 633-nm Laser at very low power, in the temperature range of 4-330 K [33-34]. To the best of our knowledge, hitherto there is no report on this DP system probing underlying quantum spin fluctuations and exploring the link with the anticipated spin fractionalization a necessary denominator of the quantum liquid $|GS\rangle$. The fluctuation-dissipation theorem connects the underlying dynamic fluctuations to the imaginary part of the corresponding susceptibility which is reflected in the Raman scattering. Figure 1(a) shows the imaginary part of the susceptibility

(i.e., Raman response, which reflects the dynamic properties of the collective underlying excitations) $\chi''(\omega, T)$, obtained from the observed Raman intensity $[\propto [1+n(\omega)]\chi''(\omega, T)]$ by dividing it by the Bose factor $[1+n(\omega)]$, as a function of frequency (Raman shift) for different temperature. It is very clear from the spectra that the narrow phonon modes are superimposed on the slowly varying continuum. Systematic analysis of this continuum may provide the information about the underlying long wavelength dynamical spin and/or orbital fluctuations via the dynamic Raman susceptibility. The Raman response shows a significant buildup of the intensity below $\sim 800 \text{ cm}^{-1}$ (100 meV) on lowering the temperature [see Fig. 1(a) and its inset], surprisingly only with a slight decrease upon entering into the spin solid phase. This characteristic scattering feature is typical of the scattering from underlying quantum spin fluctuations. To make a quantitative estimate, here, we focus on the dynamic Raman susceptibility ($\chi_{dyn.}(q=0, T) = \lim_{\omega \rightarrow 0} \chi(\omega, q=0, T)$) which is obtained from the Raman response at finite frequency using the Kramers-Kronig relation [35]:

$$\chi^{dyn}(q=0, T) = \frac{2}{\pi} \int_0^{\Omega} \frac{\chi''(\omega, T)}{\omega} d\omega \quad \text{-----} \quad (1)$$

The dynamic susceptibilities obtained by integrating the finite frequency responses up to Ω (= 30 meV) after subtracting the phonon response, the upper cutoff value is chosen as 30 meV, where Raman conductivity $\chi''(\omega, T)/\omega$ [see Fig. 1(b)] shows no change with further increase in the energy, are shown as a function of temperature in Fig. 1(c). With decreasing temperature χ^{dyn} shows nearly temperature independent behavior down to $\sim 240\text{-}250$ K, and upon further cooling it keeps increasing down to ~ 25 K, and below 25 K it decreases mildly till 4 K. As in the paramagnetic phase, spins are expected to have no correlation, and χ^{dyn} should be

temperature independent. The significant build of χ^{dyn} in the temperature range of ~ 250 K to ~ 25 K demonstrate the finite entanglement of spin and orbital DoF in the spin gas phase, hinting that this characteristic temperature (~ 250 K) corresponds to crossover from a conventional paramagnet to the quantum liquid state. Our results clearly suggest the strong growth of the dynamic quantum fluctuations associated with spin and orbital DoF in the paramagnetic phase, which are only mildly quenched below T_N as opposed to a conventional magnetic system, where fluctuations quenched to zero quickly below T_N in the ordered phase [36] and decay exponentially fast above T_N . In system with quantum liquid state the dynamic correlation function may show peculiar temperature and frequency dependence even below the temperature where static correlations saturate [5-7]. Recently, it was advocated that the dynamical spin fluctuations in the paramagnetic state are strongly influenced by the fractionalization of quantum spins [5], therefore the signature of quantum spin fractionalization may be visible in the dynamical measurable properties such as Raman susceptibility. Specifically, it was shown that the dynamical structure factor, which is related to the spin correlation factor exhibits emergence of a low energy quasi-elastic response at low temperature, and is postulated as smoking gun evidence for the fractionalized spins in QSL state. The emergence of a quasi-elastic peak at low energy in our measurements evince the presence of fractionalized spins deep into the paramagnetic phase signaling the quantum spin liquid state. This anomalous temperature evolution and the distinctive symmetry (to be discussed later) of this low frequency quasi-elastic peak cannot be captured by the conventional long-range magnetic scattering, rather it evinces its intimate links to the underlying spin-orbital entangled quantum liquid phase, seemingly consistent with the theoretical predictions for a QSL state. Temperature evolution of $\chi^{dyn}(T)$ [see Fig. 1(c)], above T_N is fitted well using a canonical Curie-Weiss law of the form

$\chi^{dyn}(T) = \frac{\Delta}{T-T_0}$, where Δ is a constant, and the estimated absolute Curie-Weiss temperature T_0 is ~ 55 K and is quite higher than T_N suggesting that it is free from the effects of the long-range magnetic ordering.

We also did our measurements with the different incident photon energy [see inset of Fig. 1(c)], the temperature dependence of $\chi^{dyn}(T)$ is found to be independent of the incident photon energy. This invariance of $\chi^{dyn}(T)$ suggests that the resonant terms in the Raman vertex does not modify the temperature behavior of the dynamic susceptibility response, and supporting the use of the effective mass approximation [31, 35]. In a system where both spin and orbital DoF are entangled, as in the present case, then both DoF are expected to be contribute to the total Raman response of the system. In such cases, the total Raman response $\chi''(\omega, T)$ may be given as sum of contribution from both these DoF i.e., $\chi''(\omega, T) = \chi''_{spin}(\omega, T) + \chi''_{orb./electr.}(\omega, T)$. The $\chi''(\omega, T)$ may be given as the imaginary part of the correlation function of magnetic Raman tensor and stress tensor given as [32, 35, 37-39]:

$$\chi(q, \omega) = -i \left[\int_0^\infty dt e^{i\omega t} \langle [\tau_{\alpha\beta}^+(q, t), \tau_{\alpha\beta}(0, 0)] \rangle + \int_0^\infty dt e^{i\omega t} \langle [T_{\alpha\beta}^+(q, t), T_{\alpha\beta}(q, 0)] \rangle \right] \quad \text{----- (2)}$$

where $\tau_{\alpha\beta}(r, q \rightarrow 0) = \sum_{\mu} K_{\alpha\beta\mu}(r) S_r^\mu + \sum_{\mu, \nu} G_{\alpha\beta\mu\nu}(r) S_r^\mu S_r^\nu + \sum_{\delta} \sum_{\mu, \nu} H_{\alpha\beta\mu\nu}(r, \delta) S_r^\mu S_{r+\delta}^\nu + \dots$, first

term leads to the scattering from single spin fluctuations, second and third term gives rise to the scattering by pairs of spin fluctuations. Tensor K , G and H describes the strength of the

coupling between the incident light and underlying magnetic DoF. $T_{\alpha\beta}(q) = \sum_{q, \sigma, \alpha, \beta} \gamma_{\alpha\beta}(q) C_{q\alpha\sigma}^+ C_{q\beta\sigma}$

is the stress tensor, and Raman vertex, $\gamma_{\alpha\beta}(q)$, within the effective mass approximation, valid in

non-resonant case, as here, is given as $\gamma_{\alpha\beta}(q \rightarrow 0) = \frac{1}{\hbar^2} \sum_{r,s} e^i_r \frac{\partial^2 \epsilon_k^{\alpha\beta}}{\partial k_r \partial k_s} e^f_s$, where e^i and e^f are the polarization vector of the incident and scattered light, respectively. For our experimental geometry, the incident and scattered light is confined within the XY plane, we have $e^i = \frac{1}{\sqrt{2}}(\hat{x} + \hat{y}) = e^s$; for this symmetry configuration one expect Raman vertex, $\gamma_{\alpha\beta}(q)$, to be same for both A_g and B_g symmetry i.e., orbital fluctuations may be seen in both these channel, hence the Raman response will be invariant, and is consistent with our experiments [see Fig. 1(d)]. Also, in a recent report it was suggested that the orbital fluctuations may be observed in both A_{1g} and B_{1g} channel for D_{4h} point group [28], which may be translated to A_g and B_g for C_{2h} point group in the present case. Due to the lack of local order parameter a very weak or no polarization dependence magnetic Raman response is advocated to be one of the key signatures of QSL state [40-41]. The nearly isotropic behavior of Raman response [see Fig. 1(d)] agree very well with the suggestion based on theoretical calculations. We note that, there is one caveat in our polarization dependent response i.e., we have used the polycrystals for our measurements. Probably, the single crystal studies may be more detailed; however, we note that the phonon modes show correct polarization dependence evidencing that nearly polarization invariant behavior of the continuum is intrinsic to the system.

Now, we discuss the frequency and temperature dependence of this polarization invariant response. As is clear from the spectra [see Fig. 1(a)], this fluctuations response may be decomposed into two contributions, a quasi-elastic peak in the low frequency regime (below $\sim 200 - 300 \text{ cm}^{-1}$), and a broad continuum. To quantify the temperature dependences of these two components contributing to the dynamic fluctuations, we fit the data using the following general

expression [26, 29]: $\chi''(\omega, T) = \chi''_{QEP}(\omega, T) + \chi''_b(\omega, T)$, where the first part, i.e., quasi-elastic peak (QEP) is modeled by a damped Lorentzian:

$$\chi''_{QEP}(\omega, T) = A_1(T) \frac{\Gamma(T)\omega}{\omega^2 + \Gamma^2(T)} \quad \text{----- (3)}$$

where A_1 is the quasi-elastic scattering amplitude, and Γ is the fluctuation rate. And the broad continuum, $\chi''_b(\omega, T)$, is fit using a third-order polynomial with only odd powers in ω to guarantee causality i.e., $\chi''_b(\omega, T) = B_1(T)\omega + B_2(T)\omega^3$. As is clear from Fig. 2(a) above equation fits well the Raman response data at low energy, up to $\sim 400 - 500 \text{ cm}^{-1}$. Figure 2(b) shows the temperature dependence of the inverse of A_1 and linewidth, Γ , of the QEP. The characteristics of this QEP may be linked to the mass, $M(T)$, in the fluctuation propagator [35, 42]. At temperatures, where quantum fluctuations dominate, the mass $M(T)$, inverse of spectral weight $A_1(T)^{-1}$ and the fluctuation rate, $\Gamma(T)$, are linear in T i.e., $A_1(T)^{-1} \propto (T - T^*)$ and $\Gamma(T) \propto (T - T^{**})$. In the ordered state $M(T)$ saturate, hence the extrapolation to zero of the linear part of $A_1(T)^{-1}$ may provide a good estimate of T^* . Following this, the temperature dependences of $A_1(T)$ and $\Gamma(T)$ was fitted between 60 and 130 K using a linear form $A_1^{-1} = \alpha_1(T - T^*)$ and $\Gamma = \Gamma_0(T - T^{**})$ [see solid lines in Fig. 2(b)]. Experimentally, the absolute T^* is found to be 55 K similar to T_0 , as obtained from the canonical Curie-Weiss fit of the dynamic susceptibility, $\chi^{dyn}(T)$. However, the zero-temperature intercept of the QEP linewidth, Γ , absolute T^{**} is significantly higher (145 K). One expect that both these temperature should be in similar range, the difference between T^* and T^{**} may be understood

by the temperature dependence of the quasiparticle scattering rate $\Gamma_0(T)$, which may be gauged via transport measurements. We note that the low energy QEP is well reproduced by a damped

Lorentzian, especially above ~ 60 K, $\chi''_{QEP}(\omega, T) = A_1(T) \frac{\Gamma(T)\omega}{\omega^2 + \Gamma^2(T)}$. $A_1(T)^{-1}$ extrapolating

to zero close to T_0 , and the fluctuation rate, $\Gamma(T)$, which is linked to the relaxational dynamics of the fluctuations of QEP shows a strong softening with decreasing temperature [see Fig. 2(b)].

The temperature evolution of $A_1(T)$ matches qualitatively with the $\chi^{dyn}(T)$, suggesting that the temperature dependent behavior is dominated by this low frequency QEP.

We also analyzed the data from a different perspective i.e., by carefully extracting the fluctuation part, after subtracting the continuum, which is almost constant. Interestingly, we qualitatively found that the temperature dependence is dominated by the fluctuation part which is reflected in the similarity of the temperature evolution of the low energy spectrum in the different analysis performed earlier. To extract the contribution of fluctuations, we followed the following procedure. Figure 1(a) shows the temperature evolution of Raman response, $\chi''(\omega, T)$, for $\text{Gd}_2\text{ZnIrO}_6$. The initial slope $\tau_0(T)$ [see Fig. 1(a)], using memory function method, may be related with static transport relaxation rate $\Gamma_0(T) [\equiv \Gamma_0(\omega \rightarrow 0, T)]$ of the electrons as

$$\hbar[\tau_0(T)]^{-1} = \Gamma_0(T) = \left(\frac{\partial \chi''(\omega, T)}{\partial \omega} \right)^{-1} \Bigg|_{\omega=0} \quad [43-45].$$

Figure 3(a) shows that above ~ 220 - 240 K, $\Gamma_0(T)$ is nearly constant. Below 200 K it starts decreasing, and is simultaneously accompanied by the increase in the intensity gain of the spectrum below ~ 200 - 300 cm^{-1} [see Fig. 1(a)]. We note that similar temperature dependence changes are also reflected in the $\chi^{dyn}(\omega, T)$ [see Fig. 1(c)]. This increase in the intensity with decreasing temperature points that an additional

contribution other than the continuum is building up in the background and have its origin in the fractional quantum spin fluctuations, and potentially signal the transition from the high temperature paramagnetic phase to the quantum liquid state below ~ 220 K.

Therefore, we have used this temperature as a mark of the crossover temperature to separate the quantum fluctuations response from the nearly constant continuum. For simplicity, we have considered that above ~ 220 K contribution to the Raman response is only from the continuum and subtracted the 250 K data from all the spectra at lower temperatures. The Raman response obtained after subtraction is shown in Fig. 3(b), and it increases rapidly with decreasing temperature without any divergence. Interestingly, the fluctuating Raman response, $\chi''_{Fluc.}(\omega, T)$, does not quenched below T_N as one would expect in a conventional magnet owing to the long-range order. Rather, the intensity decreases only slightly below T_N . To gauge the quantitative temperature evolution of this fluctuating part, we estimated the dynamic Raman susceptibility from this fluctuation part, $\chi^{dyn}_{Fluc.}(\omega, T)$ [see inset of Fig. 3(d)], and it shows similar behavior as that of $\chi^{dyn}(\omega, T)$, suggesting that the temperature evolution of the Raman response is dominated by the fluctuating part only. Another way of gauging temperature dependence of the intensity of the fluctuating part may be done using the initial slope of the fluctuating Raman response [27], which is proportional to the intensity, and is expected to follow $1/T - T_0$ behavior within the mean field theory. Using $\chi''_{Fluc.}(\omega, T)$, one may extract the initial slope by plotting Raman conductivity, $\chi''_{Fluc.}(\omega, T)/\omega$, at each temperature, and the temperature dependence of the initial slope may be directly read off from graph by simply plotting Raman conductivity against a logarithmic energy scale and extrapolating the same to zero frequency [see inset of Fig. 3(d)]. We extracted the slope using the procedure described above.

Surprisingly, we find excellent agreement for temperature above T_N , and qualitatively it also matches quite well with the intensity extracted using $\chi_{Fluc.}^{dyn}(\omega, T)$.

Here, we analyzed the background having a quasi-elastic peak which gains strength with lowering temperature, along with a broad continuum, which is nearly temperature independent, using dynamic Raman response and carefully extracted the fluctuation response. Our results obtained via different analysis depicts consistent anomaly in the vicinity of the same temperature i.e., $\sim 200 - 220$ K, which is the temperature where fractionalization of the spins and onset of quantum liquid phase start. These anomalies also evinced that the underlying continuum arises mainly from the fluctuation of the spin fractionalization. In summary, our in-depth temperature, polarization and different incident photon energy dependent Raman studies demonstrates the signature of spin fractionalization in iridium-based DP Gd_2ZnIrO_6 . The anomalous emergence of a long wavelength polarization invariant quasi-elastic peak, which reflects the fluctuation of the fractionalized spins, points that these three dimensional geometrically frustrated iridium-based DP systems potentially realizes the quantum liquid state.

References:

- [1] P. W. Anderson, Mater. Res. Bull. **8**, 153 (1973).
- [2] M. R. Norman, Rev. Mod. Phys. **88**, 041002 (2016) and reference therein.
- [3] Y. Zhou et al., Rev. Mod. Phys. **89**, 025003 (2017) and reference therein.
- [4] H. Takagi et al., Nat. Rev. Phys. **1**, 264 (2019) and reference therein.
- [5] J. Yoshitake et al., Phys. Rev. Lett. **117**, 157203 (2016).
- [6] L. J. Sandilands et al., Phys. Rev. Lett. **114**, 147201 (2015).
- [7] A. Banerjee et al., Nat. Mater. **15**, 733 (2016).

- [8] W. M. H. Natori and J. Knolle, Phys. Rev. Lett. **125**, 067201 (2020).
- [9] A. Glamazda et al., Nat. Commun. **7**, 12286 (2016).
- [10] S.-H. Do et al., Phys. Rev. Lett. **124**, 047204 (2020).
- [11] B. Singh et al., Phys. Rev. Research **2**, 013040 (2020).
- [12] I. Kimchi and Ashvin Vishwanath, Phys. Rev. B **89**, 014414 (2014).
- [13] A. M. Cook et al., Phys. Rev. B **92**, 020417(R) (2015).
- [14] A. A. Aczel et al., Phys. Rev. B **99**, 134417 (2019).
- [15] M. J. P. Gingras and P. A. McClarty, Rep. Prog. Phys. **77**, 056501 (2014).
- [16] P. Kumar et al., Phys. Rev. B **85**, 134449 (2012).
- [17] B. Singh et al., J. Phys.: Condens. Matter **31**, 065603 (2019).
- [18] J. G. Rau et al., Annu. Rev. Condens. Matter Phys. **7**, 195 (2016) and reference therein.
- [19] B. Singh et al., Phys. Rev. Research **2**, 023162 (2020).
- [20] E. M. Plotnikova et al., Phys. Rev. Lett. **116**, 106401 (2016).
- [21] B. Yuan et al., Phys. Rev. B **95**, 235114 (2017).
- [22] K. Kitagawa et al., Nature **554**, 341 (2018).
- [23] M. Vogl et al., Phys. Rev. Materials **4**, 054413 (2020).
- [24] S. Gao et al., Phys. Rev. B **102**, 024424 (2020).
- [25] S. Hüfner, Optical Spectra of Transparent Rare Earth Compounds (Academic Press, New York, 1978).
- [26] S. Yoon et al., Phys. Rev. Lett. **85**, 3297 (2020).
- [27] F. Kretzschmar et al., Nat. Phys. **12**, 560 (2016).
- [28] H. Yamase and R. Zeyher, Phys. Rev. B **88**, 125120 (2013).
- [29] P. Massat et al., Proc. Nat. Aca. Sci. **113**, 9177 (2016).

- [30] N. Nagaosa and P. Lee, Phys. Rev. B **43**, 1233(R) (1991).
- [31] B. S. Shastry and B. I. Shraiman, Phys. Rev. Lett. **65**, 1068 (1990).
- [32] T. P. Devereaux and R. Hackl, Rev. Mod. Phys. **79**, 175 (2007).
- [33] B. Singh et al., J. Phys.: Condens. Matter **31**, 395701 (2019).
- [34] D. Kumar et al., J. Phys.: Condens. Matter **31**, 505403 (2019).
- [35] Y. Gallais and I. Paul, C. R. Phys. **17**, 113 (2016).
- [36] W. Hayes and R. Loudon, Scattering of light by crystals, Dover New York (2004).
- [37] G. F. Reiter, Phys. Rev. B **13**, 169 (1976).
- [38] M. G. Cottam and D. J. Lockwood, Light scattering in magnetic solids, Wiley, New York (1986).
- [39] T. Moriya, J. Phys. Soc. Japan **23**, 490 (1967).
- [40] O. Cépas et al., Phys. Rev. B **77**, 172406 (2008).
- [41] J. Knolle et al., Phys. Rev. Lett. **113**, 187201 (2014).
- [42] S. Caprara et al., Phys. Rev. Lett. **95**, 117004 (2005).
- [43] M. Opel et al., Phys. Rev. B **61**, 9752 (2000).
- [44] W. Götze and P. Wölfle, Phys. Rev. B **6**, 1226 (1972).
- [45] J. W. Allen and J. C. Mikkelsen, Phys. Rev. B **15**, 2952 (1977).

Acknowledgment

PK thanks IIT Mandi for the experimental facilities and DST India for the financial support. The authors at Dresden thank Deutsche Forschungsgemeinschaft (DFG) for the financial support via Grant No. DFG AS 523/4-1 (S.A.) and via project B01 of SFB 1143 (project-id 247310070).

FIGURE CAPTION:

FIGURE 1: (Color online) **(a)** Temperature evolution of the Raman response $\chi''(\omega, T)$ (obtained raw Raman intensity/ $1+n(\omega)$]). Inset shows the phonons subtracted Raman response at selected temperature. **(b)** Temperature dependence of the phonons subtracted Raman conductivity $\chi''(\omega, T)/\omega$. **(c)** Temperature dependence of the dynamic Raman susceptibility χ^{dyn} , extracted using the Kramer-Kronig relation

$$\chi^{dyn}(q=0, T) = \frac{2}{\pi} \int_0^{\Omega} \frac{\chi''(\omega, T)}{\omega} d\omega; \text{ by integrating the finite frequency responses up to } \Omega = 30$$

meV). Inset shows the dynamic susceptibility at different excitation energy i.e., 1.96 eV (633-nm). The solid line above T_N is a Curie-Weiss fit to the Raman dynamic susceptibility as described in the text. **(d)** Polarization dependence of the prominent phonon modes (at ~ 83.5 meV), and Raman response after subtraction of the phonons along with the dynamic Raman susceptibility.

FIGURE 2: (Color online) **(a)** Low energy fits using a damped Lorentzian, and an odd in frequency polynomial to the Raman susceptibility [i.e., $\chi''(\omega, T) = \chi''_{QEP}(\omega, T) + \chi''_b(\omega, T)$;

where $\chi''_{QEP}(\omega, T) = A_1(T) \frac{\Gamma(T)\omega}{\omega^2 + \Gamma^2(T)}$ and $\chi''_b(\omega, T) = B_1(T)\omega + B_2(T)\omega^3$]. **(b)** Temperature

dependence of the inverse of the area $A_1(T)$ and linewidth $(\Gamma(T))$ of the quasi-elastic peak. The solid lines are the linear fits between 60 K and 130 K.

FIGURE 3: (Color online) **(a)** Raman relaxation rates $\Gamma_0(T) \left[= \left(\frac{\partial \chi''(\omega, T)}{\partial \omega} \right)^{-1} \right]_{\omega=0}$ as a function of temperature. Dotted black and red lines are guide to the eye. **(b)** Fluctuation contribution to the Raman response extracted from full Raman response by carefully subtracting the response at 250 K from all the lower temperature data. **(c)** Temperature dependence of fluctuating Raman conductivity, $\chi''_{Fluc.}(\omega, T) / \omega$. **(d)** Temperature dependence of the initial slope of the fluctuating Raman conductivity extracted as described in the text. Inset shows the temperature dependence of the fluctuating dynamic Raman susceptibility $\chi_{Fluc.}^{dyn}$, extracted using the Kramer-Kronig relation $(\chi_{Fluc.}^{dyn}(q=0, T) = \frac{2}{\pi} \int_0^{\Omega} \frac{\chi''_{Fluc.}(\omega, T)}{\omega} d\omega$; by integrating the finite frequency responses up to $\Omega = 30$ meV).

Figure 1:

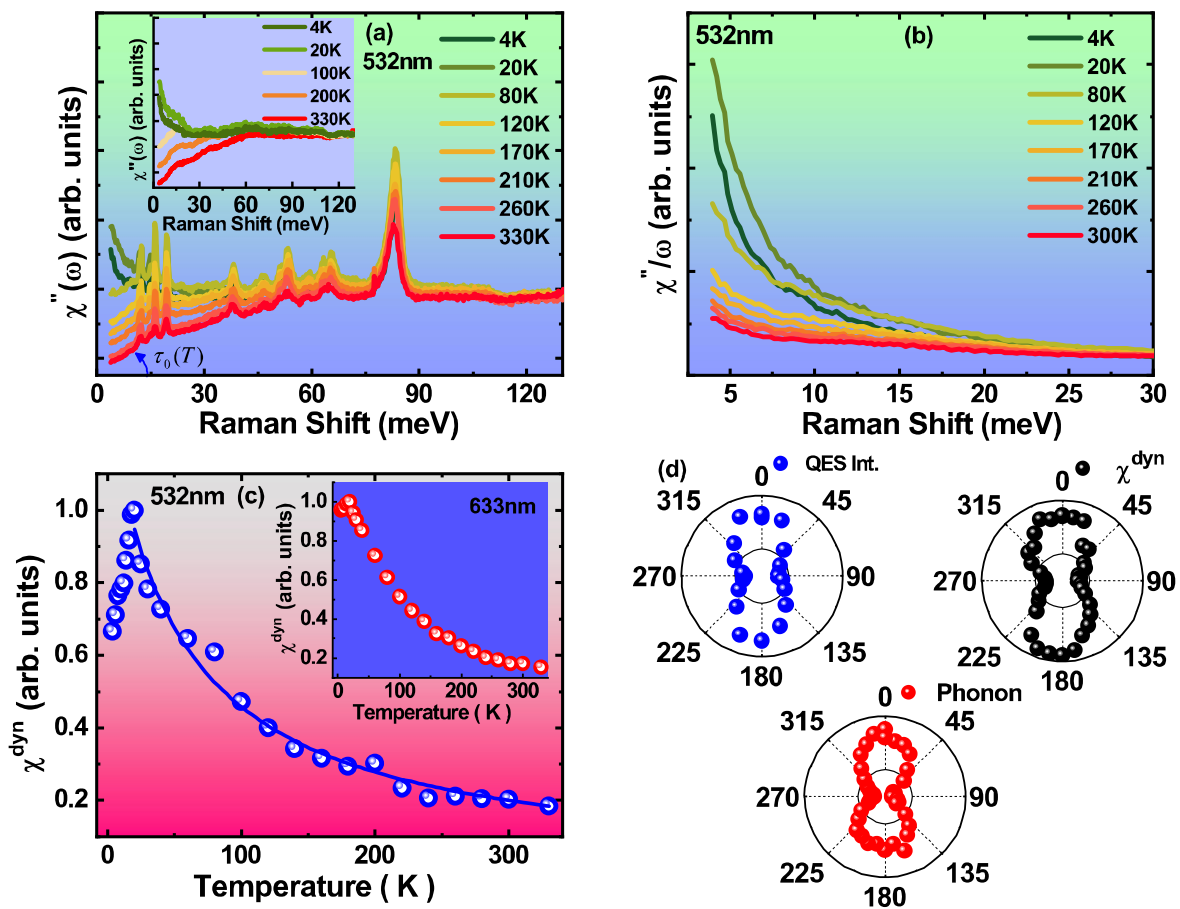


Figure 2:

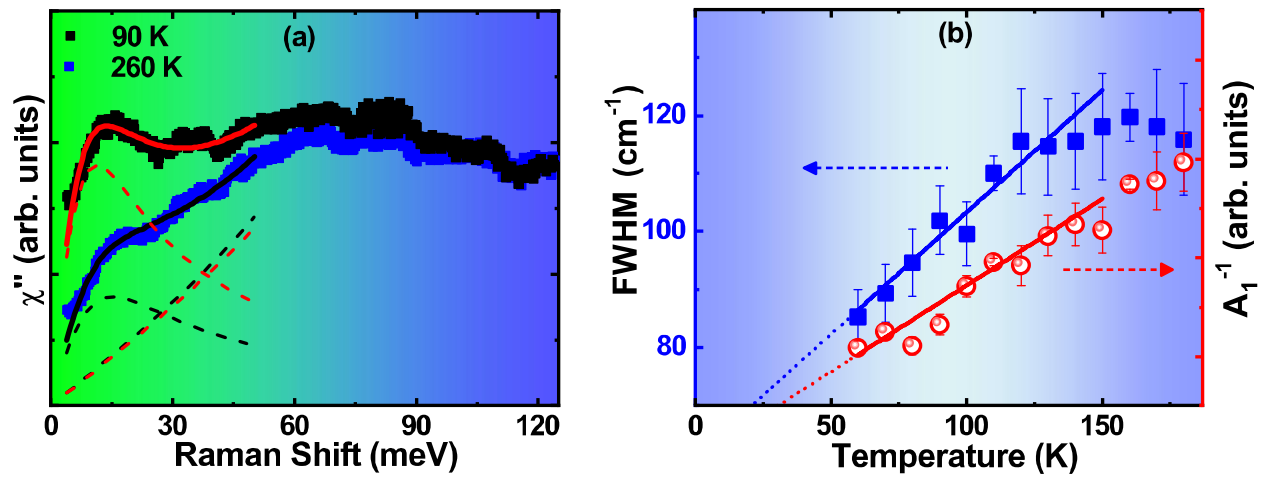


Figure 3:

